

Multi-Instrument Studies of Ionospheric Electrodynamics

Bela G. Fejer
Center for Atmospheric and Space Sciences
Utah State University
Logan, UT 84322-4405

1997 CEDAR Workshop
Boulder, CO

OUTLINE

1. Introduction
2. Quiet-Time Ionospheric Plasma Drifts.
 - Latitudinal dependence
 - Longitudinal variation
 - Altitudinal dependence
 - Quiet time variability
3. Generation Mechanisms of Storm-Time Ionospheric Electric Fields.
 - Magnetospheric dynamo and steady-state disturbance electric fields.
 - Ionospheric disturbance dynamo.
4. Equatorial, Low and Mid-Latitude Disturbance Zonal Plasma Drifts.
 - Satellite and Incoherent scatter radar drifts.
 - Comparison with results from the Rice Convection model, and from the ionospheric disturbance dynamo model.
 - Relationship to storm-time thermospheric neutral winds.
5. Summary and Conclusions.

Introduction

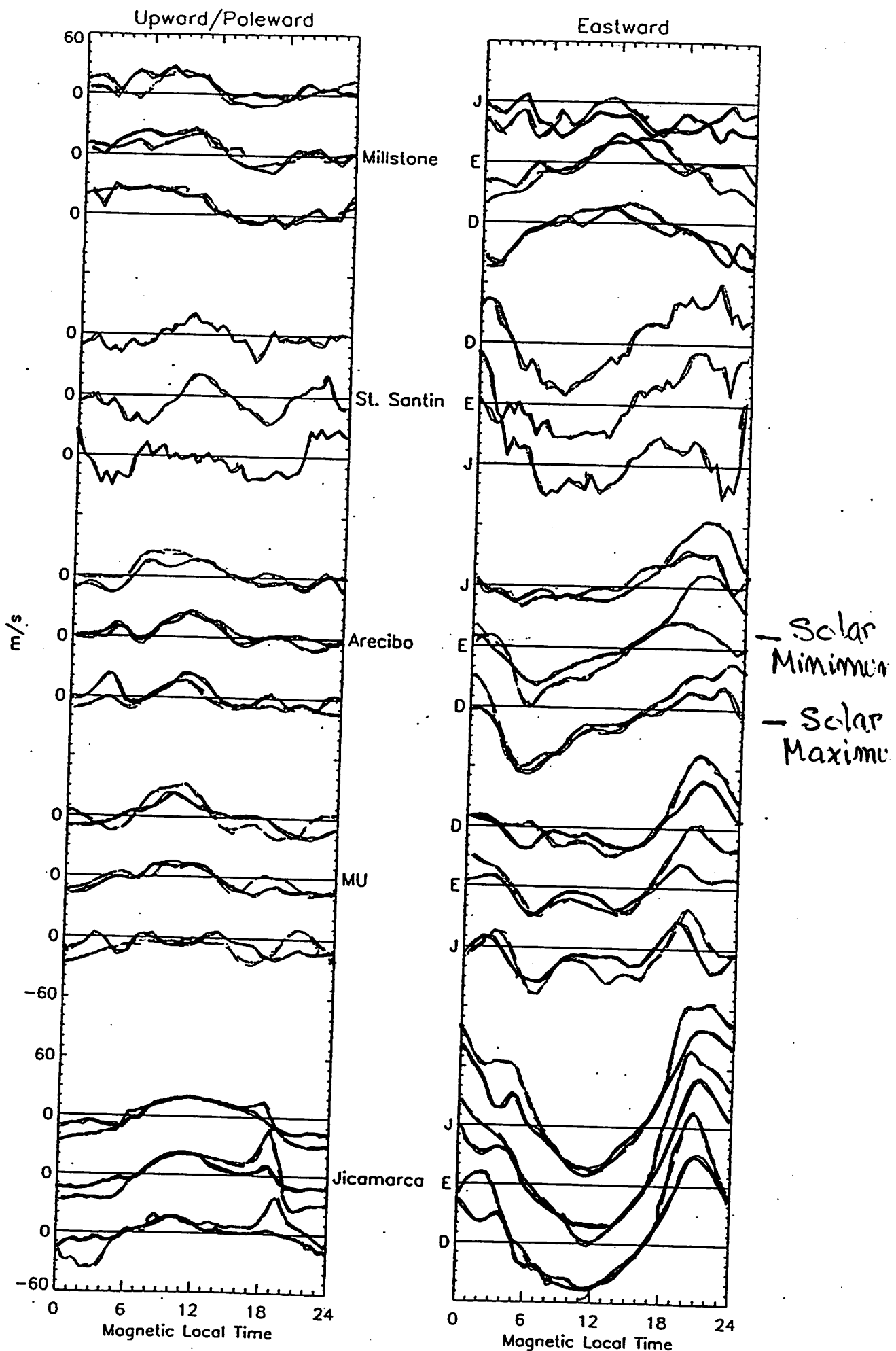
Ionospheric electric fields and plasma drifts play important roles on the distribution of ionization and dynamics of the thermosphere as well as on the generation of plasma instabilities which affect communication and radio positioning systems.

Low and Mid-latitude F-region average plasma drifts have been determined from incoherent scatter radar measurements at Jicamarca (Peru), Arecibo (Puerto Rico), at the MU radar (Shigaraki, Japan), and from Millstone Hill (Westford, MA)

In the equatorial region with ionosonde and spaced receiver observations has also been used.

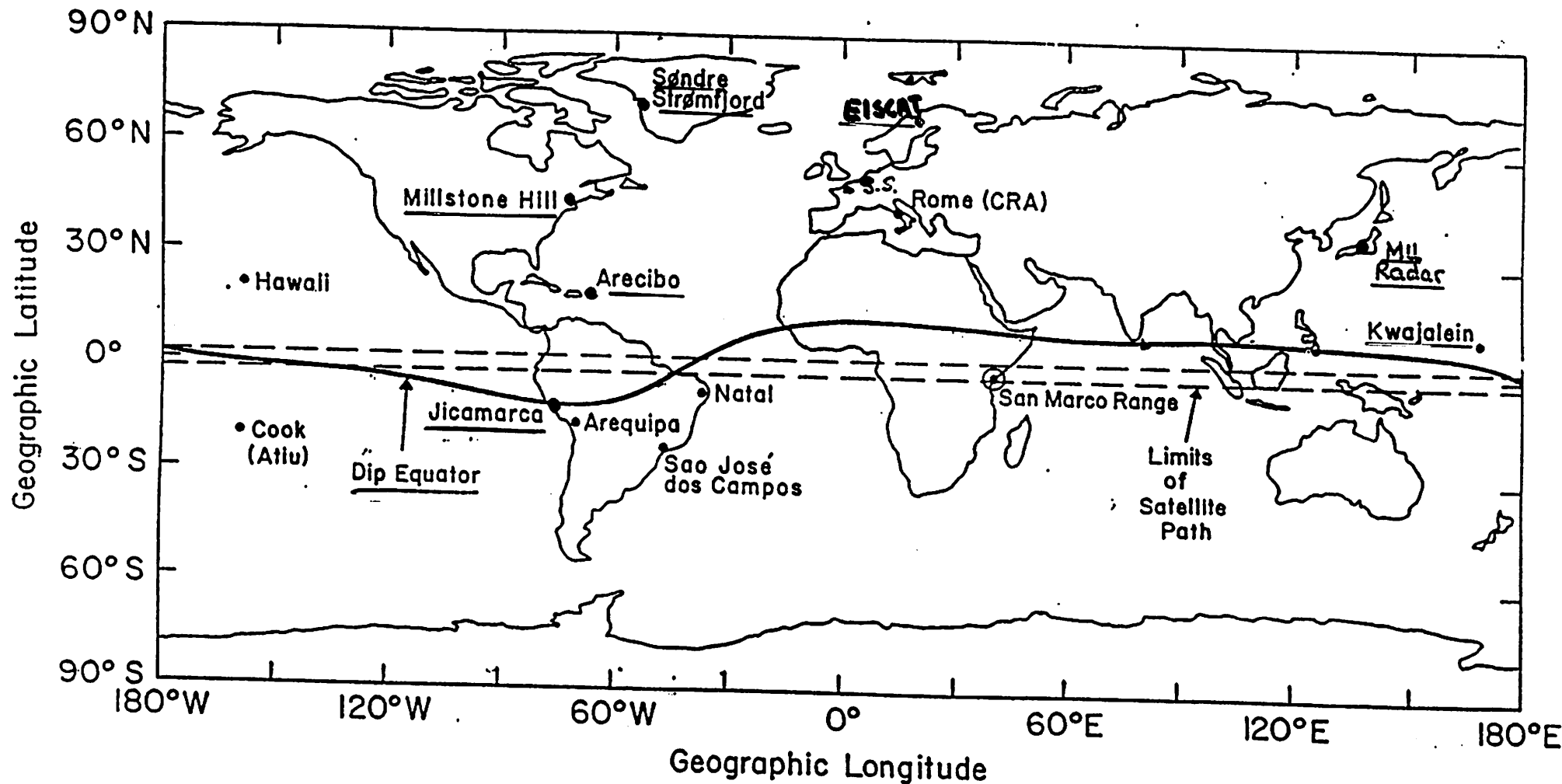
Ionospheric plasma drifts have also been studied using Ion Drift Meter (IDM) and Vector Electric Field Instrument (VEFI) data on board the AE-E, DE-2, San Marco, and Akebono satellites.

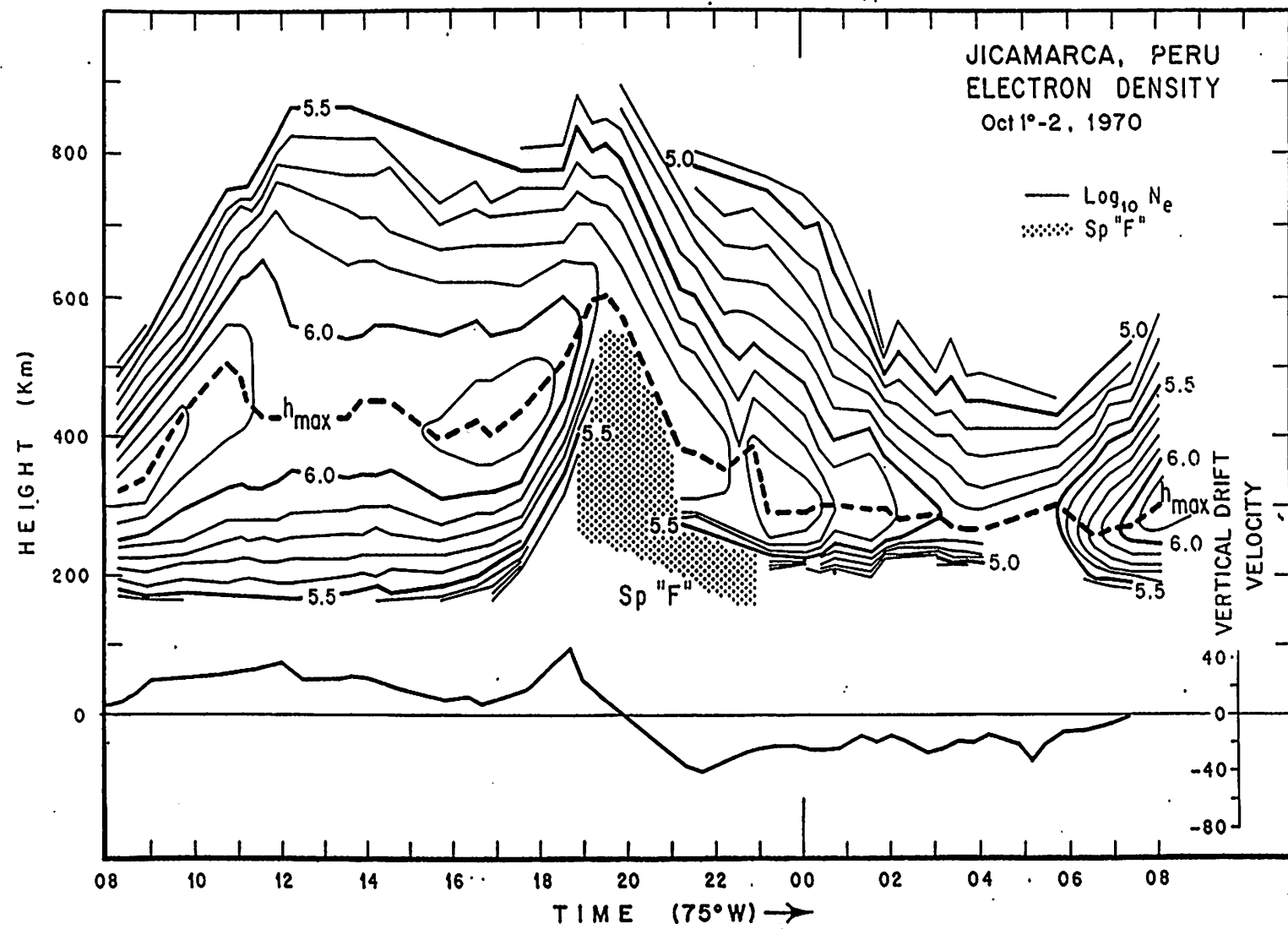
These measurements have determined the general characteristics of the average quiet-time ionospheric plasma drifts (electric fields) and, recently, also the basic signatures of magnetospheric and ionospheric disturbance dynamo electric fields. The generation and global distribution of ionospheric plasma drifts during quiet and disturbed conditions has also been investigated using global numerical models (e.g., TIEGCM, Rice Convection Model).



Richmond [1995]

SAN MARCO TRAJECTORY & MAGNETIC DIP EQUATOR (1987.0 MODEL)





$$\frac{\partial N_i}{\partial t} + \mathbf{V}_{i\perp} \cdot \nabla N_i = P_i - L_i - \nabla(N_i \mathbf{V}_{i\parallel}) - N_i \nabla \cdot \mathbf{V}_{i\perp}$$

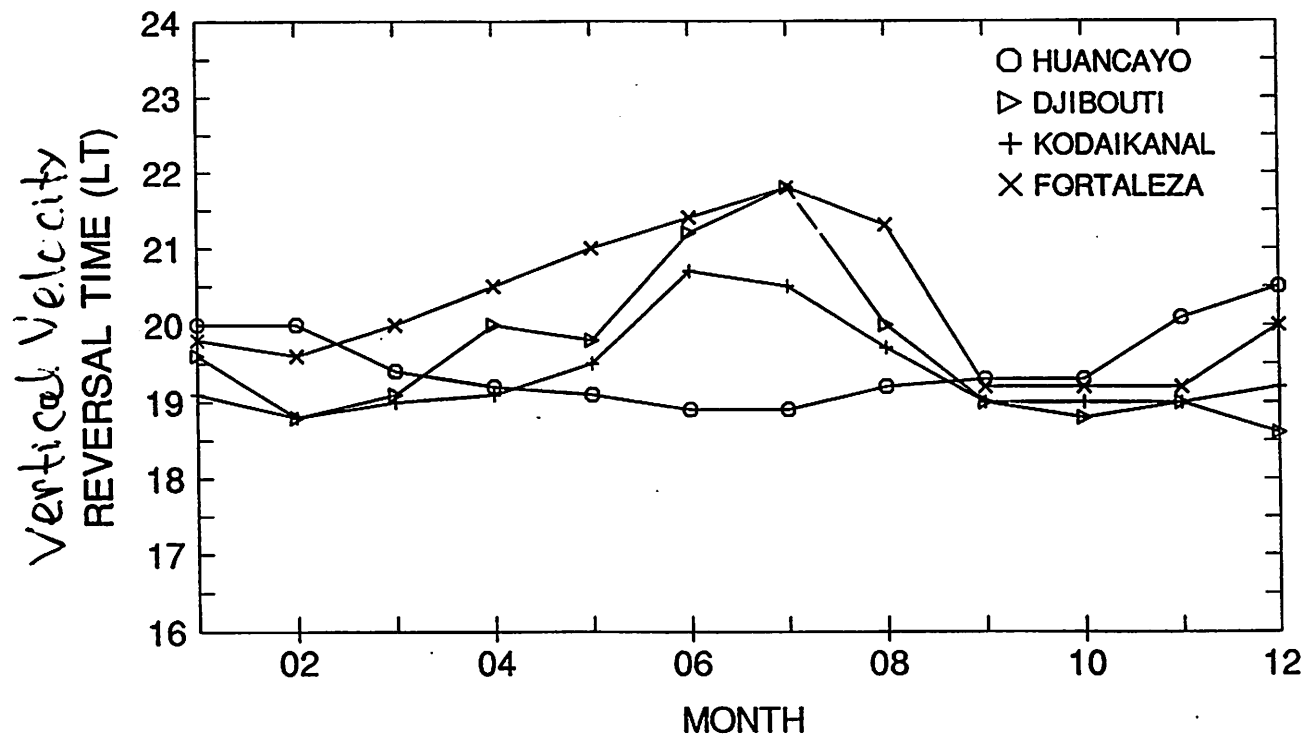
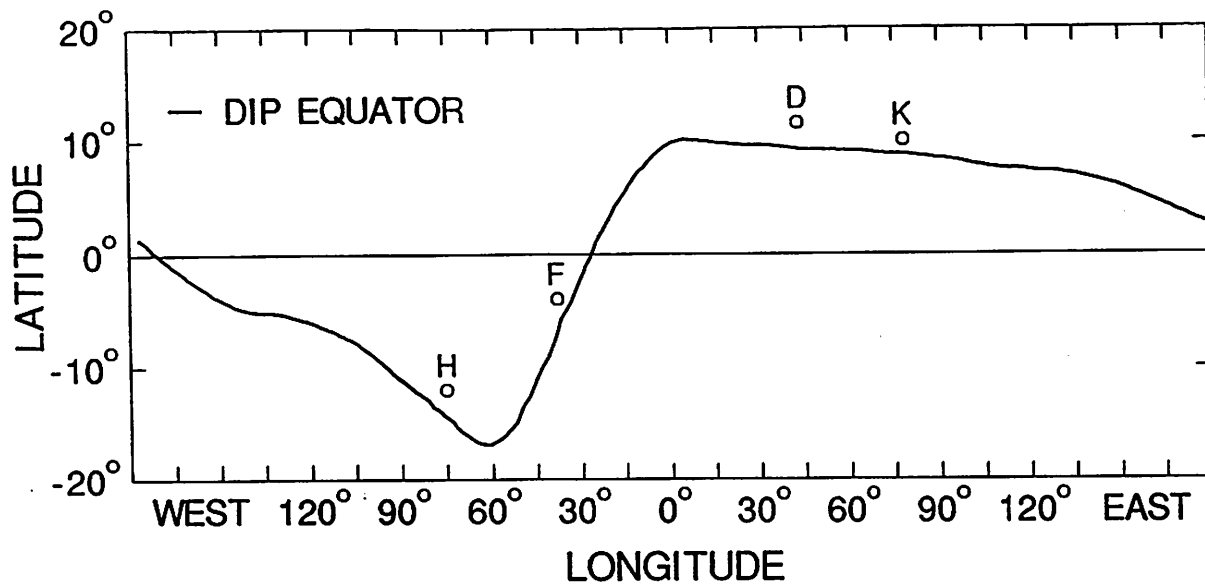
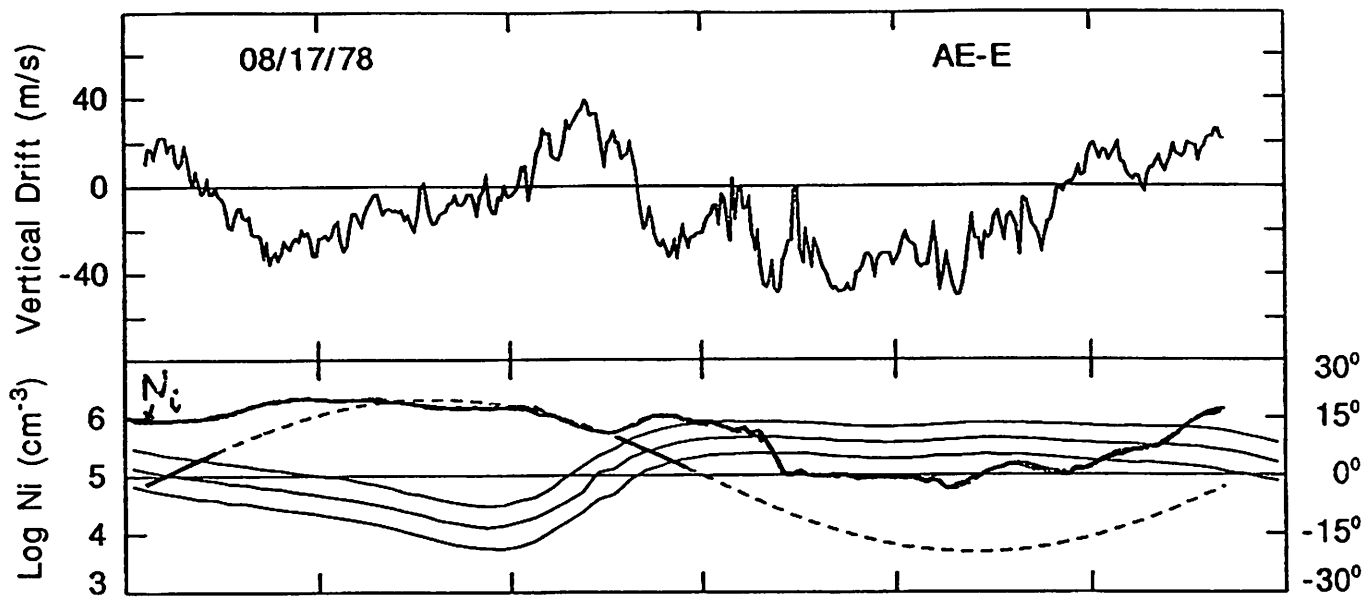
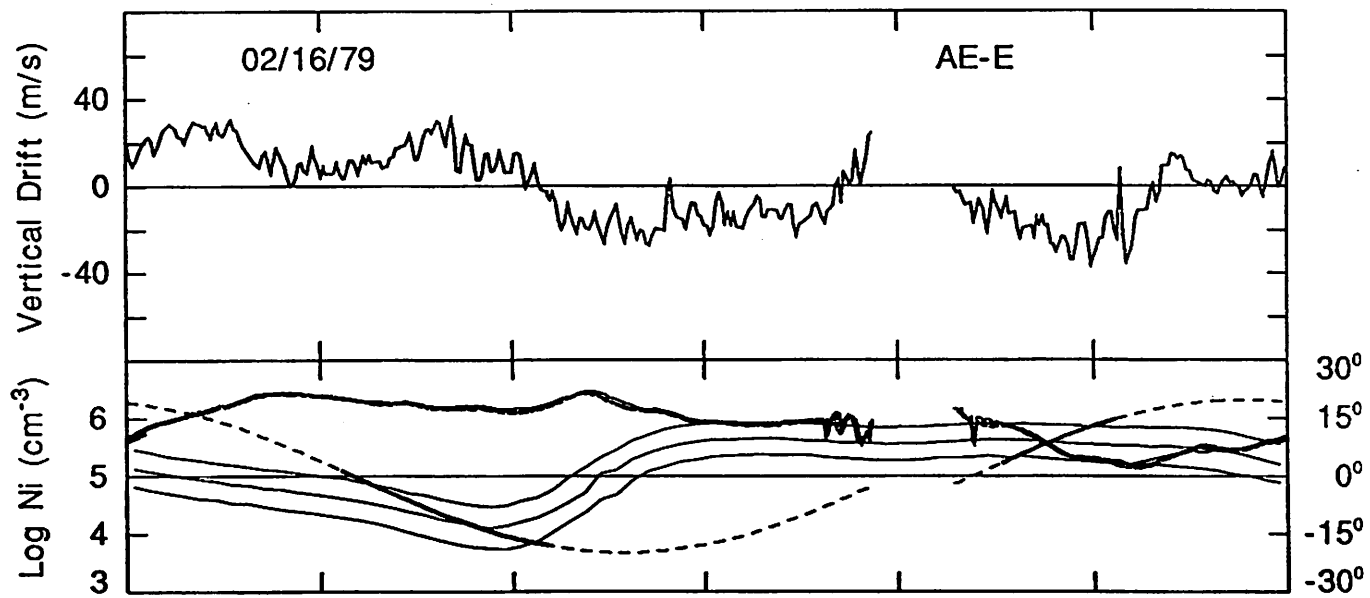


Figure 3. (a) Longitudinal variation of the location of the magnetic dip equator, (b) Evening reversal times of the equatorial vertical drifts at four stations determined from ionosonde observations [after Fejer *et al.*, 1991].



LONG	-120.0	-60.0	0.0	60.0	120.0	180.0
UT	21.48	21.74	22.02	22.30	22.56	00.00
ALT (km)	372.4	373.2	373.6	376.6	375.4	0.0
DLAT	21.0	28.8	-10.9	-31.7	-27.9	0.0
SLT	13.4	17.7	22.0	2.2	6.5	0.0



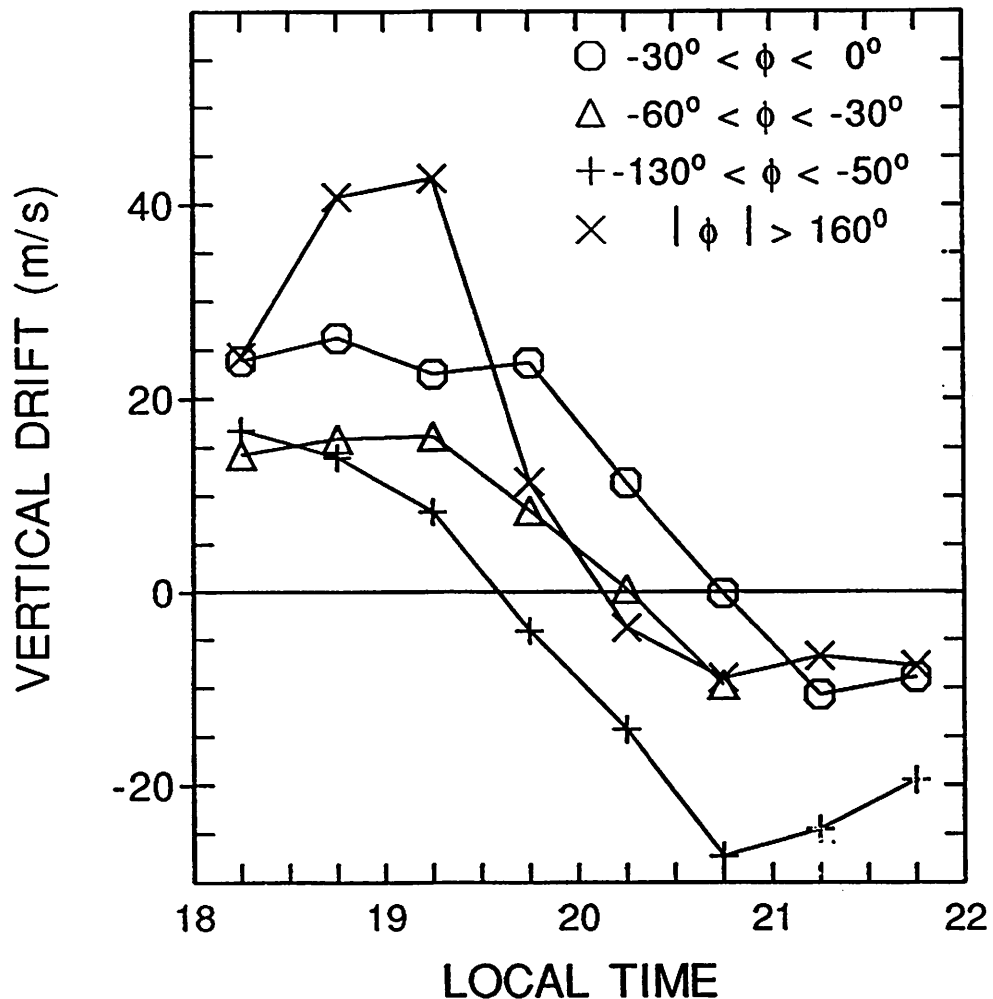
LONG	-120.0	-60.0	0.0	60.0	120.0	180.0
UT	20.92	21.21	21.48	21.73	20.38	20.64
ALT (km)	460.6	468.0	468.4	461.7	457.7	457.3
DLAT	9.0	-2.9	-29.9	-13.3	5.3	15.6
SLT	12.7	17.0	21.3	1.0	4.2	8.4

Fejer et al. 1995

The equatorial vertical plasma drifts exhibit large longitudinal effects

AE-E MAY-AUG 1978-1979 $0 \leq K_p \leq 3$

DIP LAT $\leq |5.0^\circ|$



EQUATORIAL PLASMA DRIFT

MEASUREMENT TECHNIQUES

- Jicamarca Incoherent Scatter Radar Measurements
 - Drift measurements usually between 250 and 700 km.
 - Height resolution 20-45 km, integration time \sim 5 min.
 - Height averaged vertical velocities correspond to the F region peak and above.
 - Accuracy of the height averaged velocities \sim 1-2 m/s.
- Ionosonde Drifts Measurements
 - Calculated from $\Delta(h'F)/\Delta t$.
 - Ionosonde drifts are affected by height dependent chemical loss effects when $h'F < 300$ km.
 - For $h'F < 300$ km, the upward (downward) drifts are overestimated (underestimated) by $V = \beta L$, where β is the loss coefficient and L is the electron density gradient length (about 10-50 km).
 - We use drifts from 15 min soundings and between 1700-2000 LT, when $h'F$ is above 300 km.
- AE-E IDM Drift Measurements
 - Horizontal and vertical components perpendicular to the satellite track (20° inclination) determined from the angles of arrival of ions (1° corresponding to about 140 m/s).
 - Average satellite altitudes during low, moderate and high solar flux periods were about 260, 340, 450 km.
 - Velocity measurements not reliable for low plasma densities (smaller than about 10^4 cm^{-3}).
 - Large longitudinal bins (60° - 100°) are necessary for determining seasonal and solar cycle effects.

○ JIGAMARCA * HUANCAYO $K_p \leq 3$

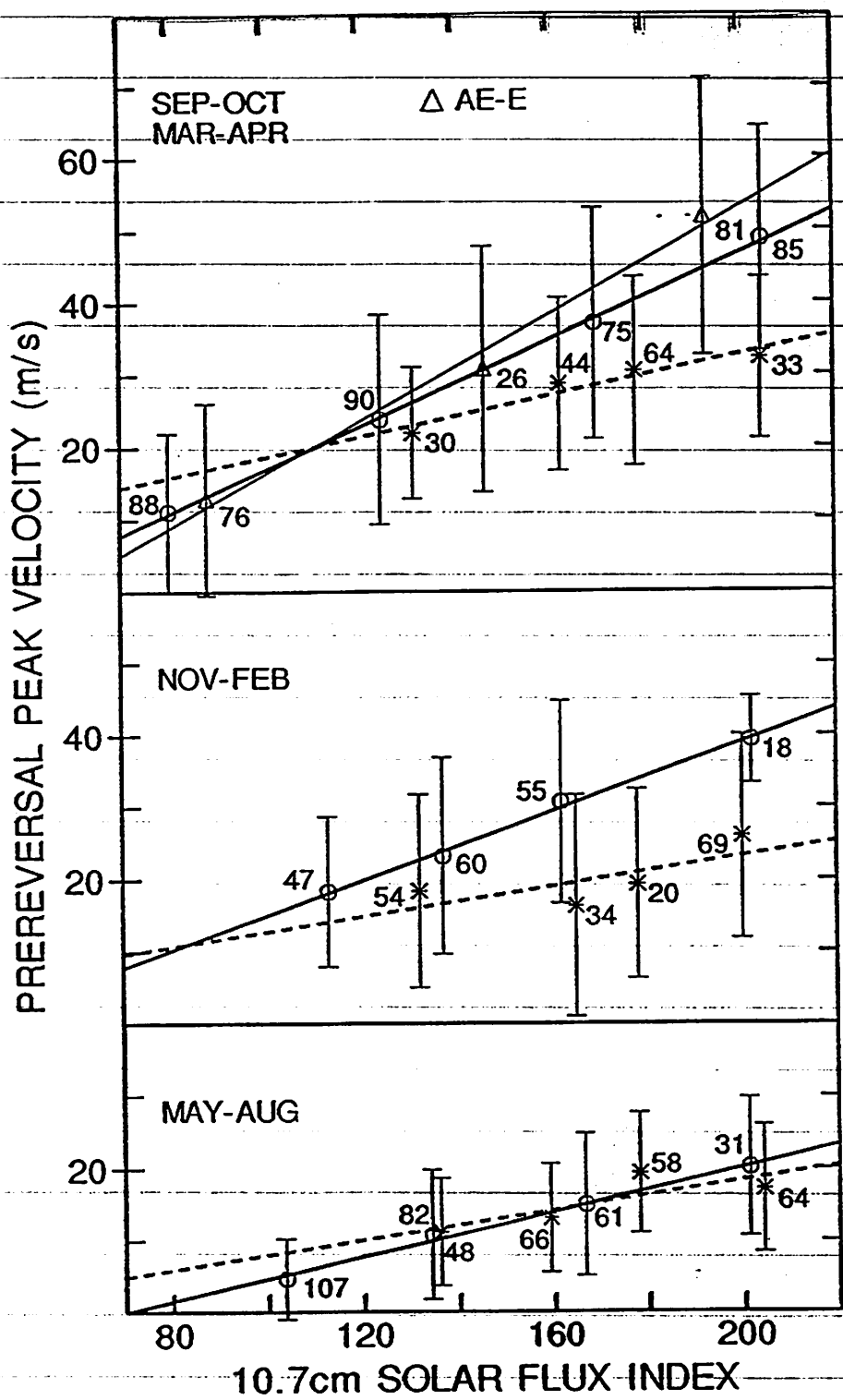
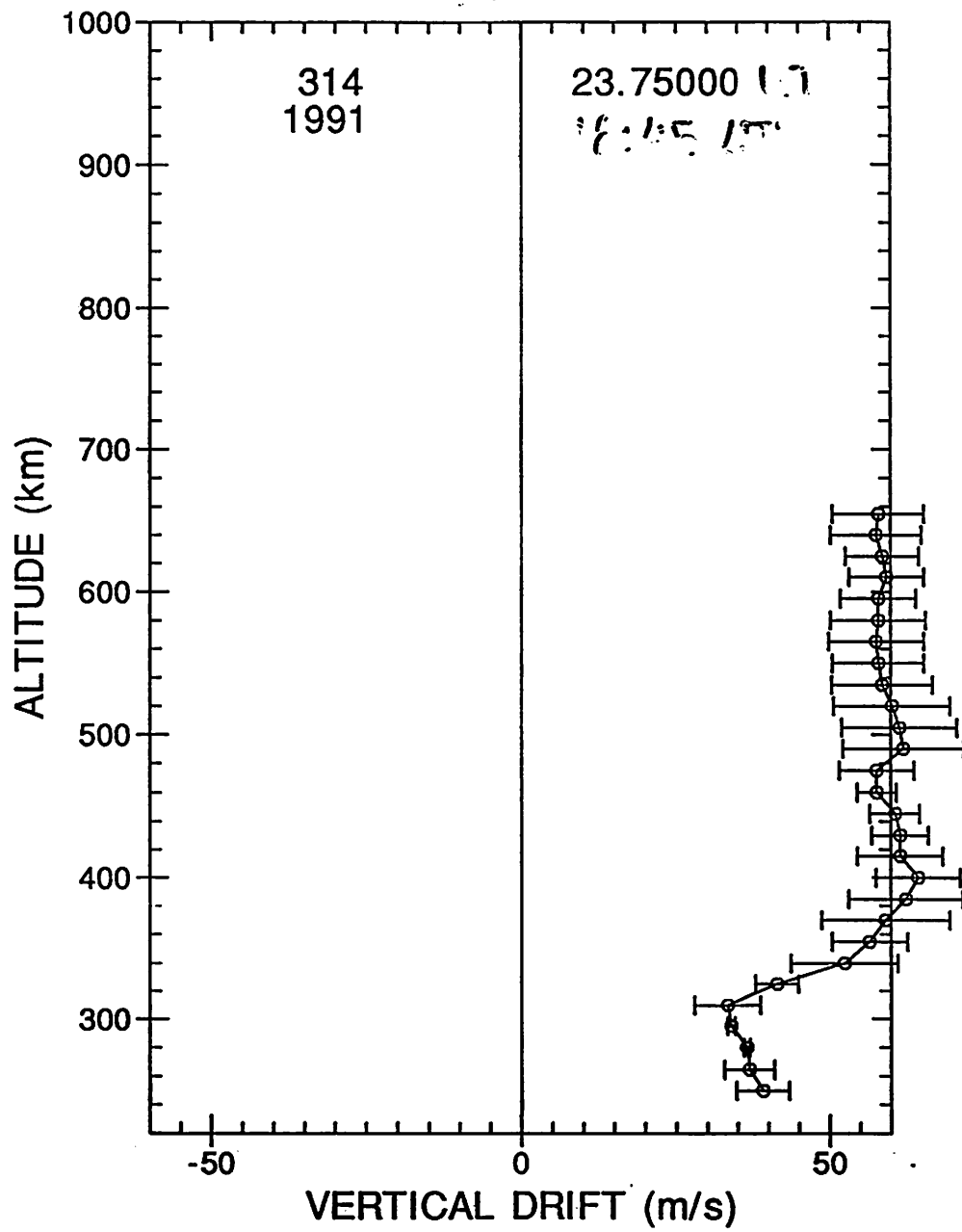
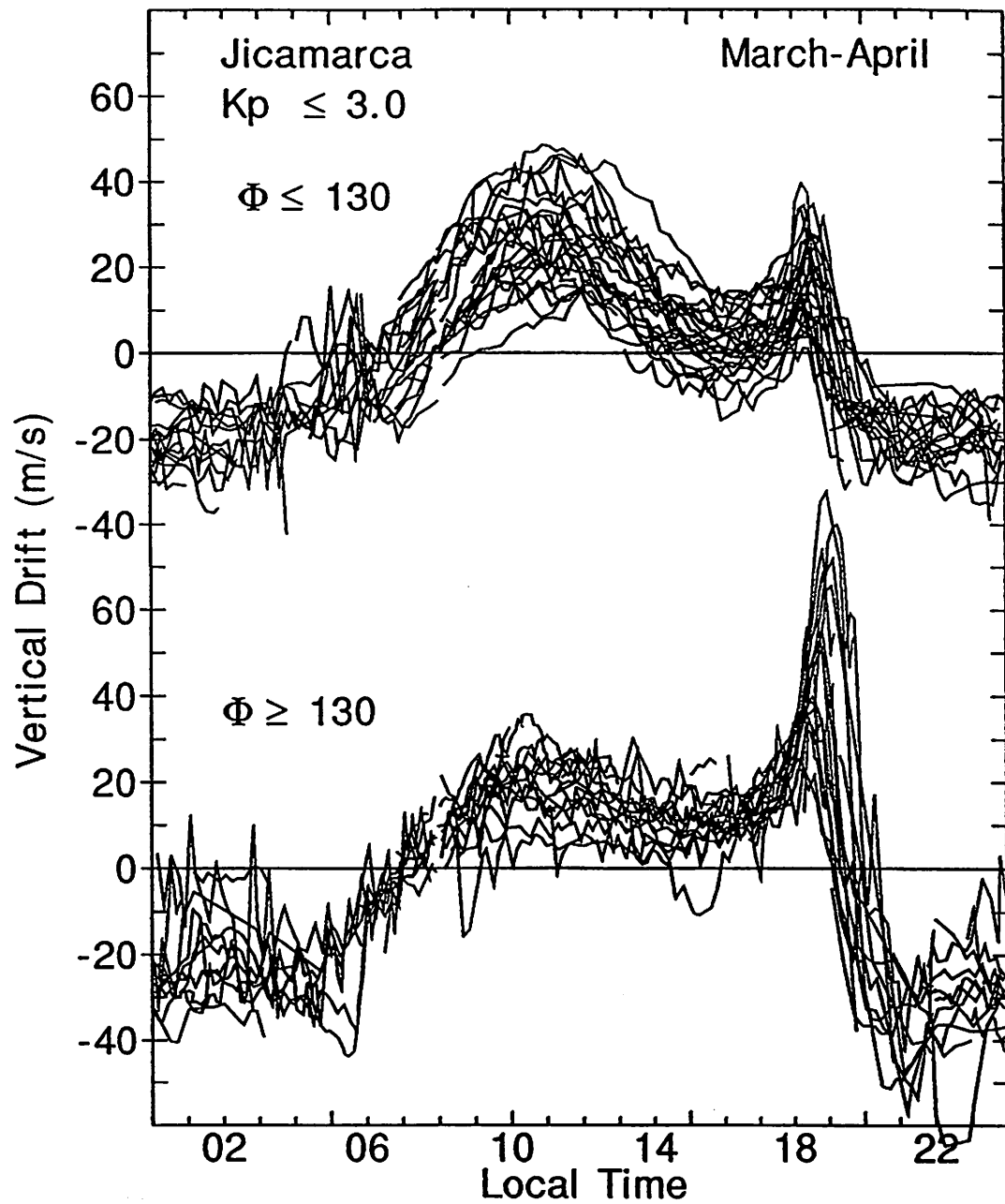


Figure 4. Variations of the radar, ionosonde, and satellite equatorial evening prereversal peak velocities over Peru with the decimetric solar flux index.

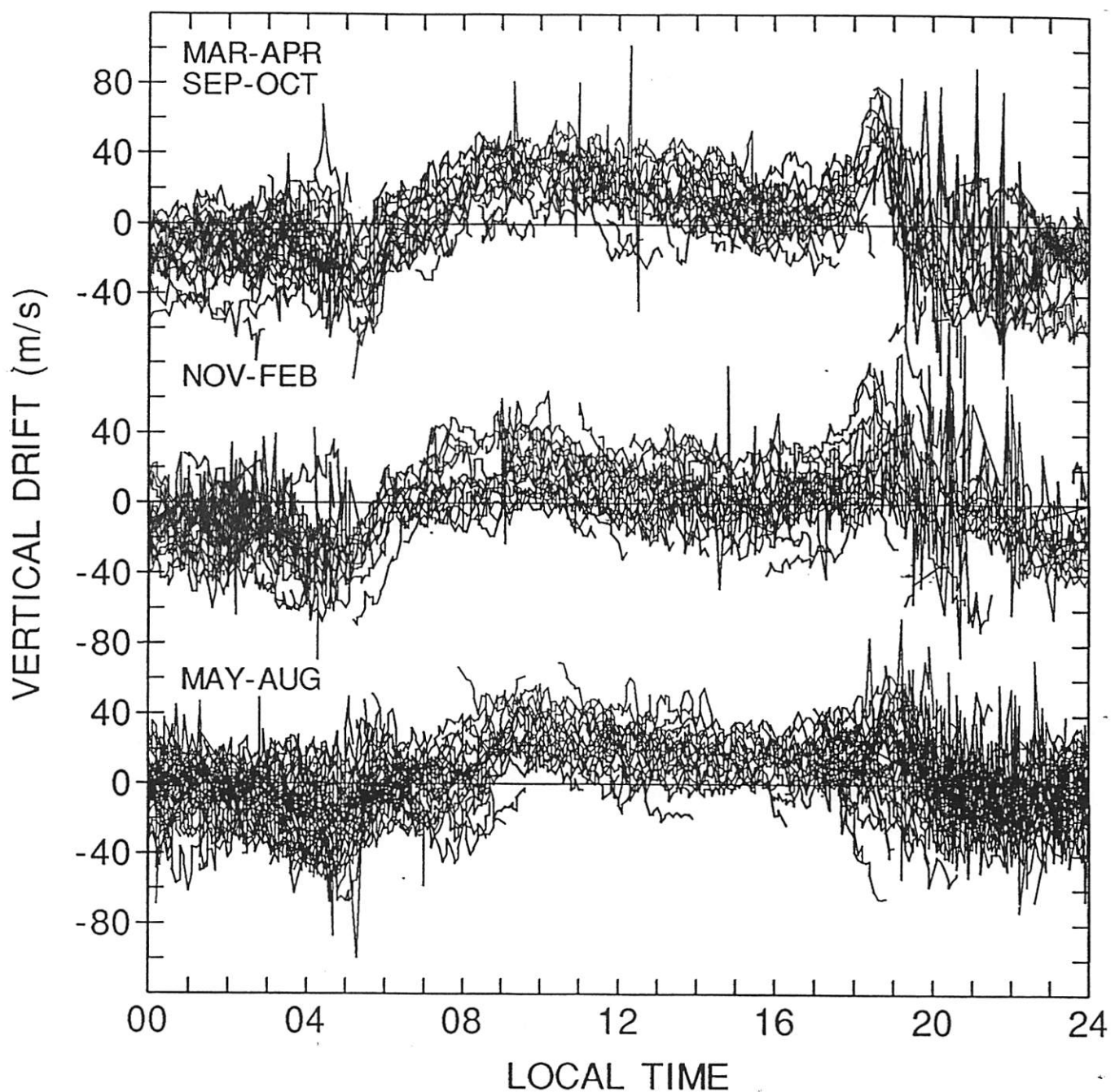
TICAMORES
14 MAY 1991



QUIET-TIME VARIABILITY



AE-E 1978-79 DIP LAT < | 7.5° |



Solar Maximum:
 $H \approx 400 \text{ km}$
AE-E
May-Aug. 1978, 79
 $-15 < \text{DIPLAT} < 15$

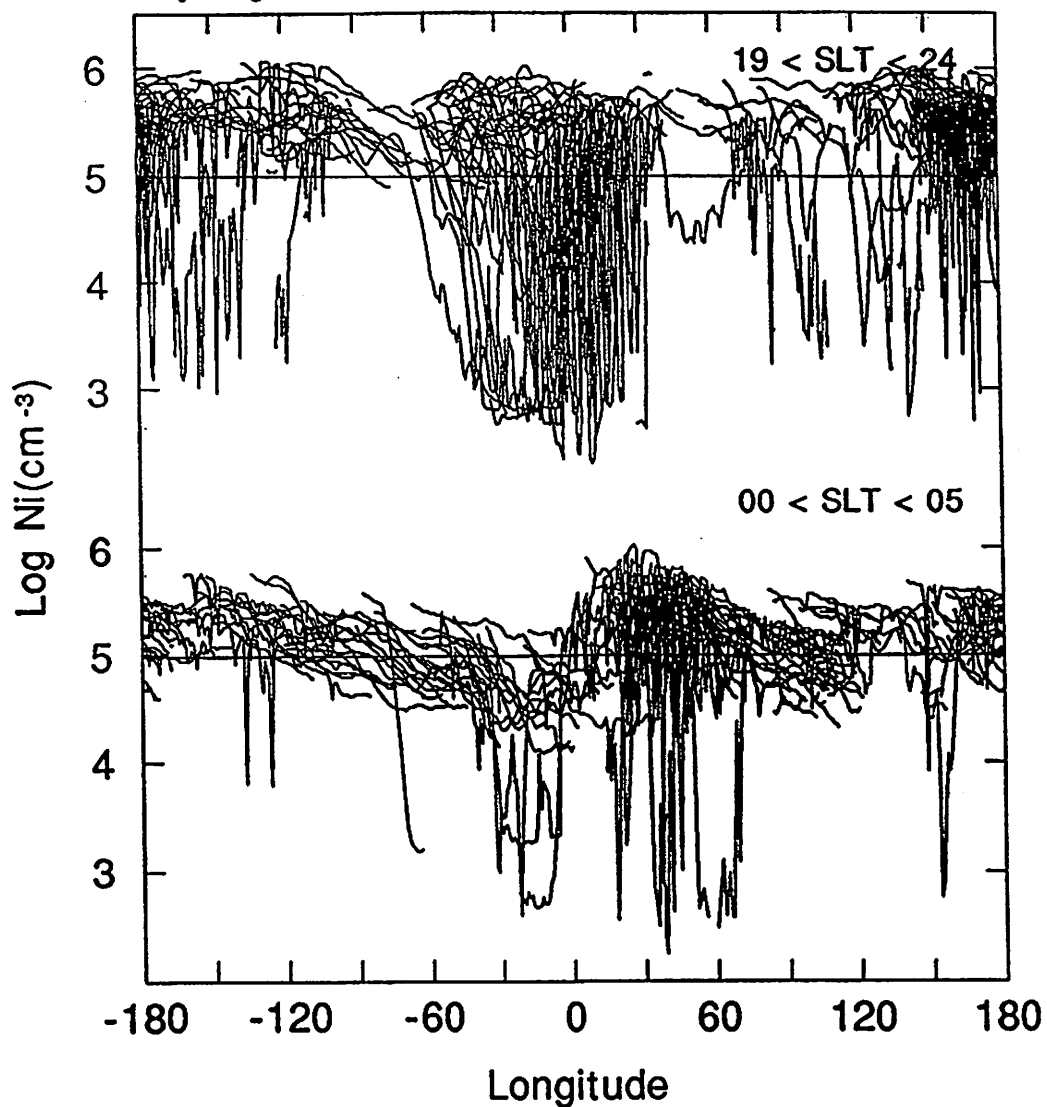
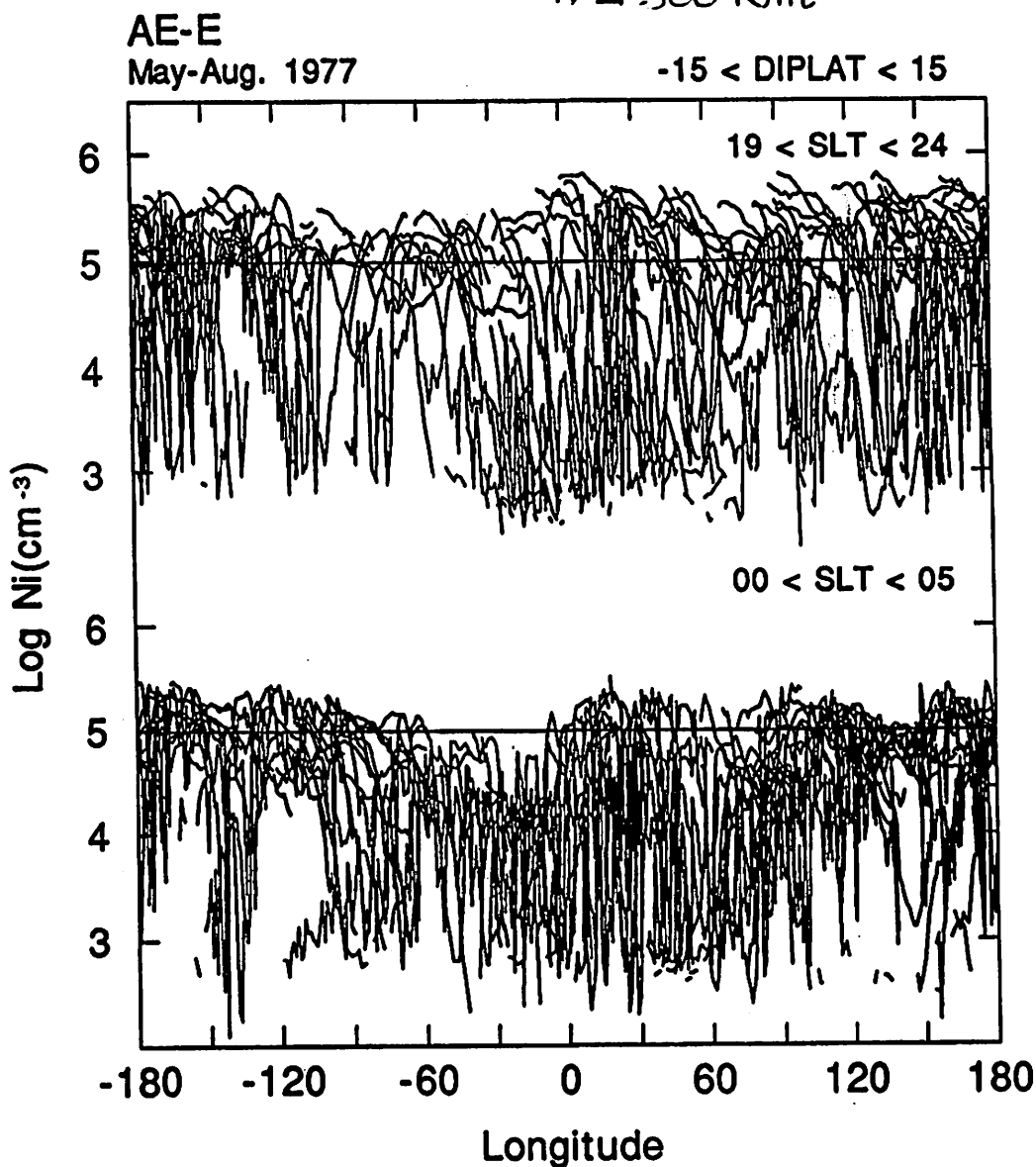


Figure 6. Longitudinal variation of electron density measured by the AE-E satellite during 1978, 1979 June solstice (May-August). Notice the large longitudinal variation of the large electron density biteouts.

Fejer, Hanson and Heelis [1983]

Solar Minimum
 $H \approx 300$ km.



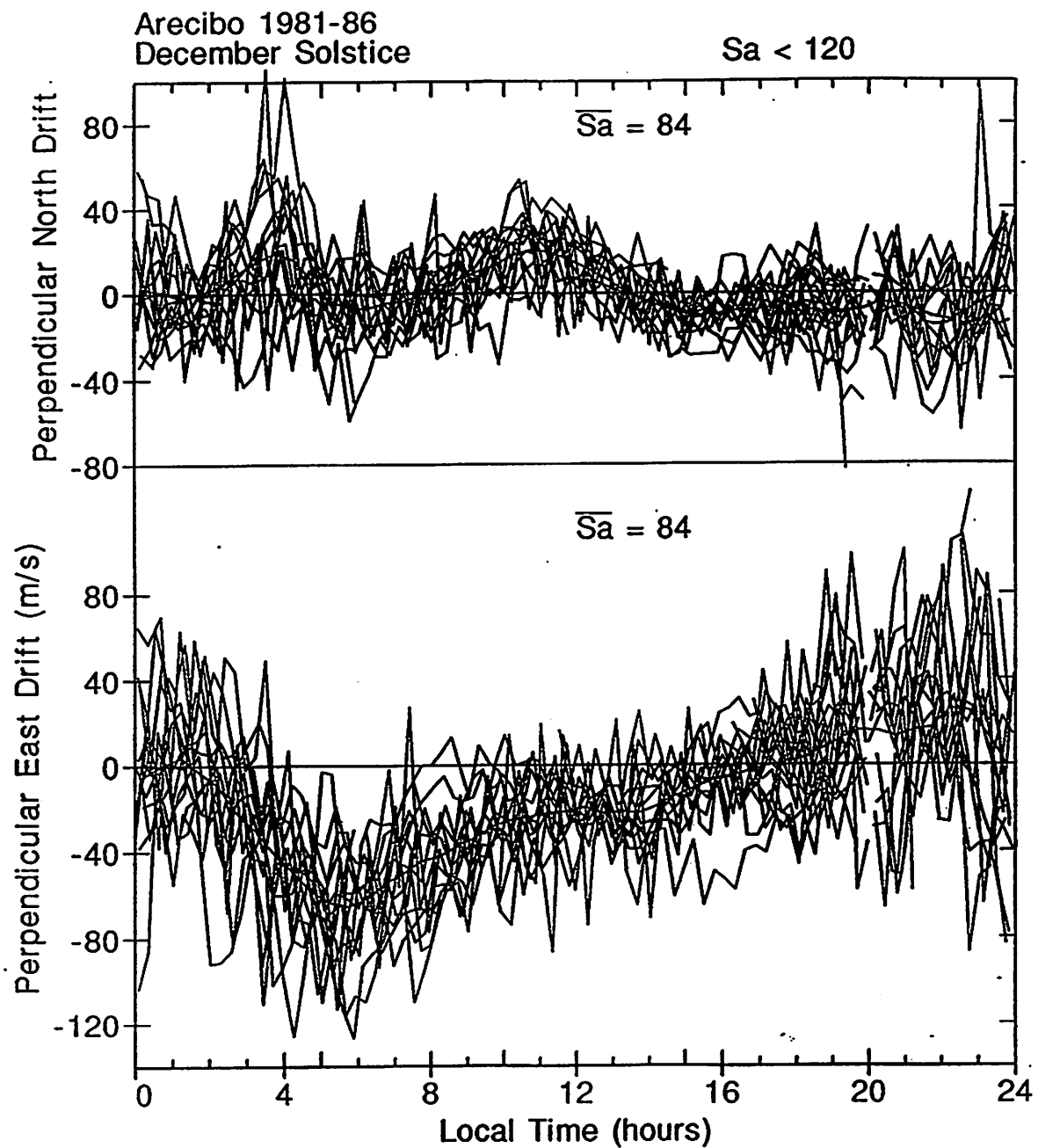


Figure 1. Scatter plots of the perpendicular north and east components of the Arecibo F region plasma drifts during magnetically quiet ($K_p \leq 3$) and solar low decimetric flux ($S_a < 120$) conditions.

DE-2
Satellite

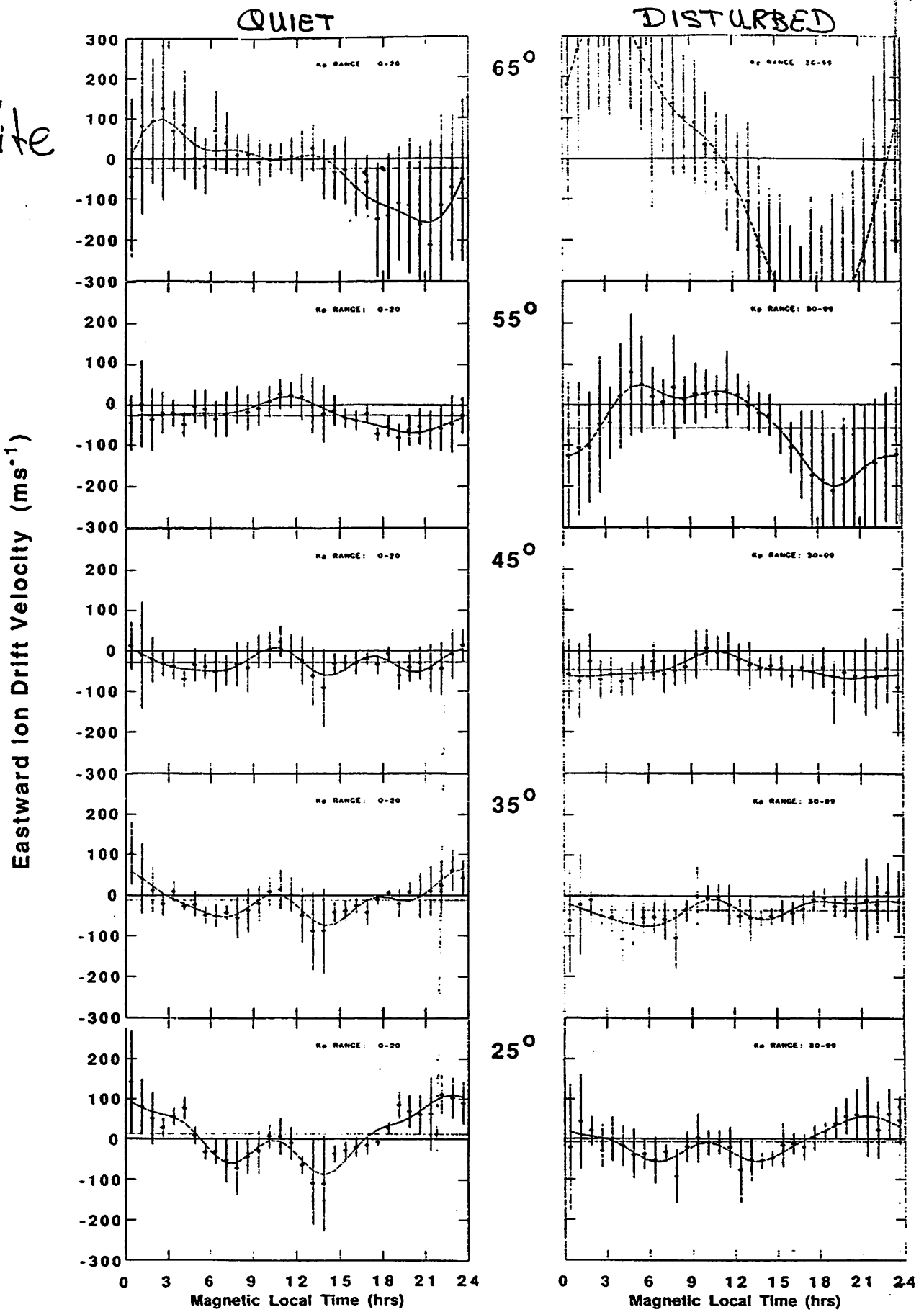


Fig. 3. Average east-west ion drifts shown as a function of local time at invariant latitudes of 65°, 55°, 45°, 35°, and 25°. Vertical bars indicate the scatter about the mean values and the solid curve is obtained from a fit to the data with a dc offset and 4 tidal components with periods of 24, 12, 8, and 6 hours. The dc offset is shown by the light dotted line.

Generation Mechanisms of Disturbance Ionospheric Electric Fields

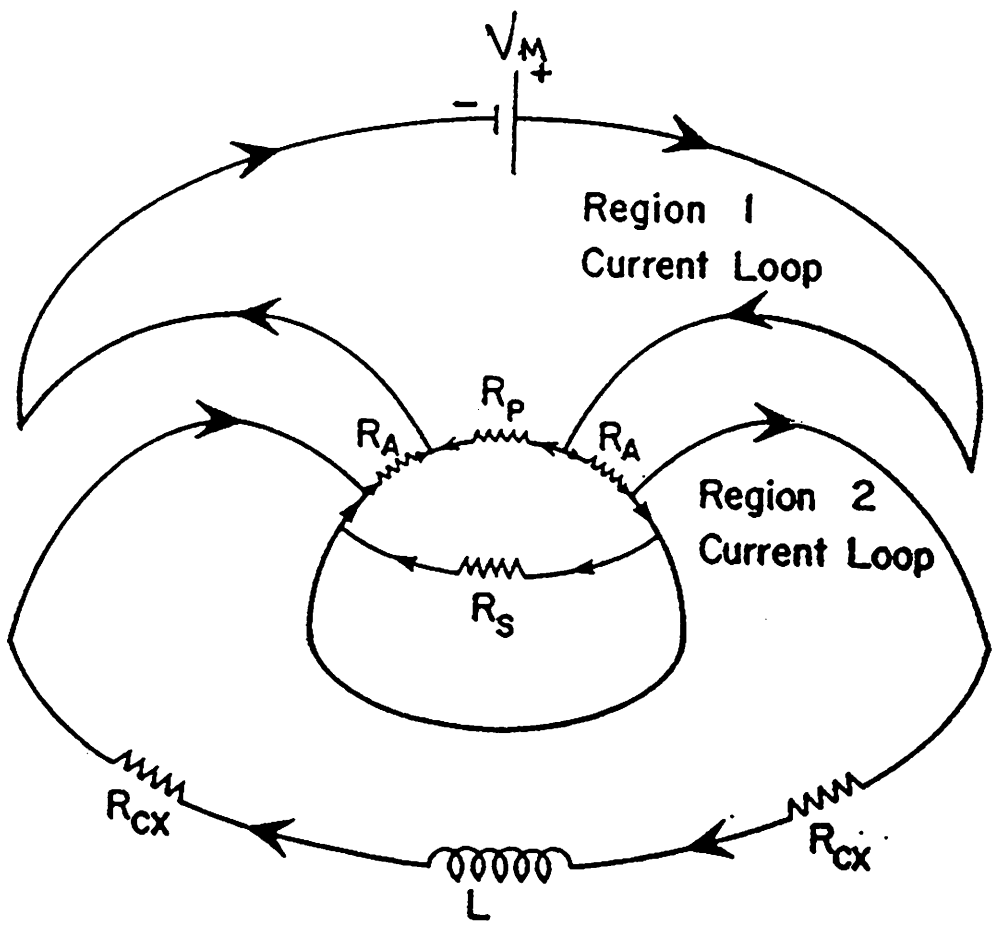
- Magnetospheric Dynamo Processes**

Electric fields due to leakage of high latitude currents into the mid and low latitude ionosphere

- Storm Time Ionospheric Dynamo**

Electric fields due to storm time winds and conductivity changes driven by large energy input (mostly Joule heating) into the high latitude ionosphere

Magnetospheric Dynamics



After Siscoe, 1992

(Riley, 1994)

Steady-State potential drop across the ~~low~~ sub-auroral ionosphere

$$V_s = \frac{\Sigma_A}{\Sigma_A + 2(\Sigma_R + \Sigma_S)} \quad R_{CZ} = \frac{1}{\Sigma_R}$$

$$R_A = 1/\Sigma_A$$

$$\text{For } \Sigma_L \ll \Sigma_A \ll \Sigma_R \quad V_s = (\Sigma_A / 2\Sigma_R) V_M$$

$$\text{Shielding time constant } \tau = L/R_S \approx \frac{\Sigma_A}{2} L_R$$

$$L_R \approx \tau_{\text{grad}} / \Sigma_R \quad \therefore \tau \approx (\Sigma_A / 2\Sigma_R) \tau_{\text{grad}}$$

τ_{grad} = drift period of a hot particle

(similar results obtained by Gonzales et al., 1993)

Disturbance Dynamo Model

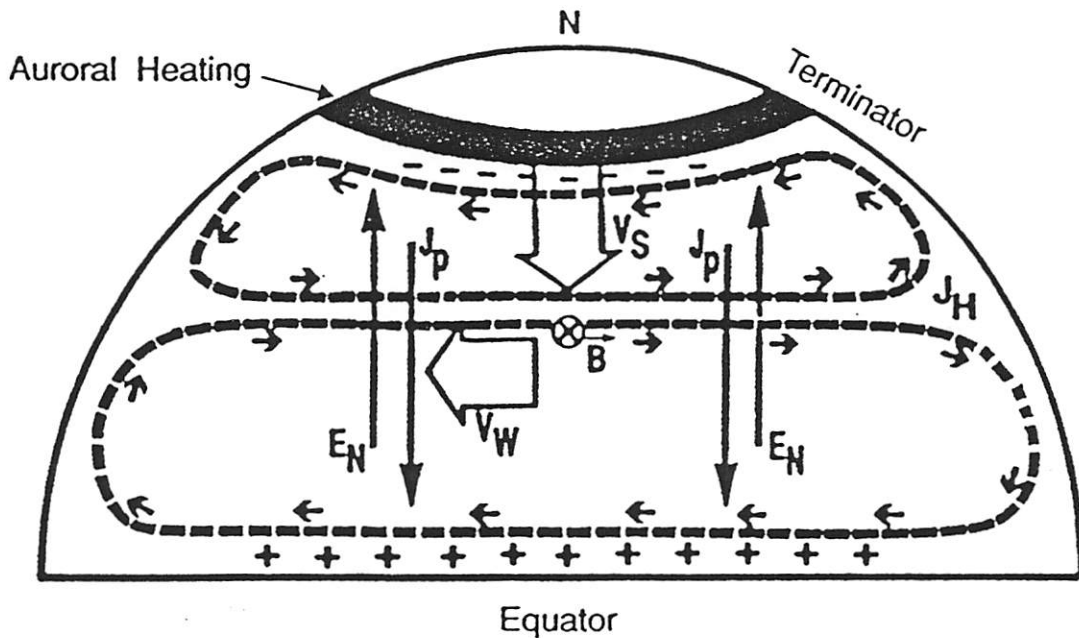


Figure 9

Schematic of the variables in the Blanc-Richmond (1980) theory. The Joule heating from the storm is assumed to extend uniformly around a high-latitude zone. The southward meridional winds at F region heights arising from this heating is shown as the arrow V_s . Due to the action of the Coriolis force, the southward meridional wind produces westward zonal motion (shown as the arrow V_w). The zonal motion of the ions in combination with the downward component of the magnetic field (shown as $\otimes B$) produces an equatorward Pedersen current (shown as J_p). The Pedersen current builds up positive charges at the equator until an electric field is established in the poleward direction opposing the flow of the Pedersen current. This poleward electric field is shown as E_N . This electric field which is perpendicular to the downward component of B gives rise to an eastward Hall current with maximum intensity in middle latitudes. This Hall current is marked as J_H . The Hall current is interrupted at the terminators and gives rise to two current vortices as shown.

Mazaudier et al. [1987]

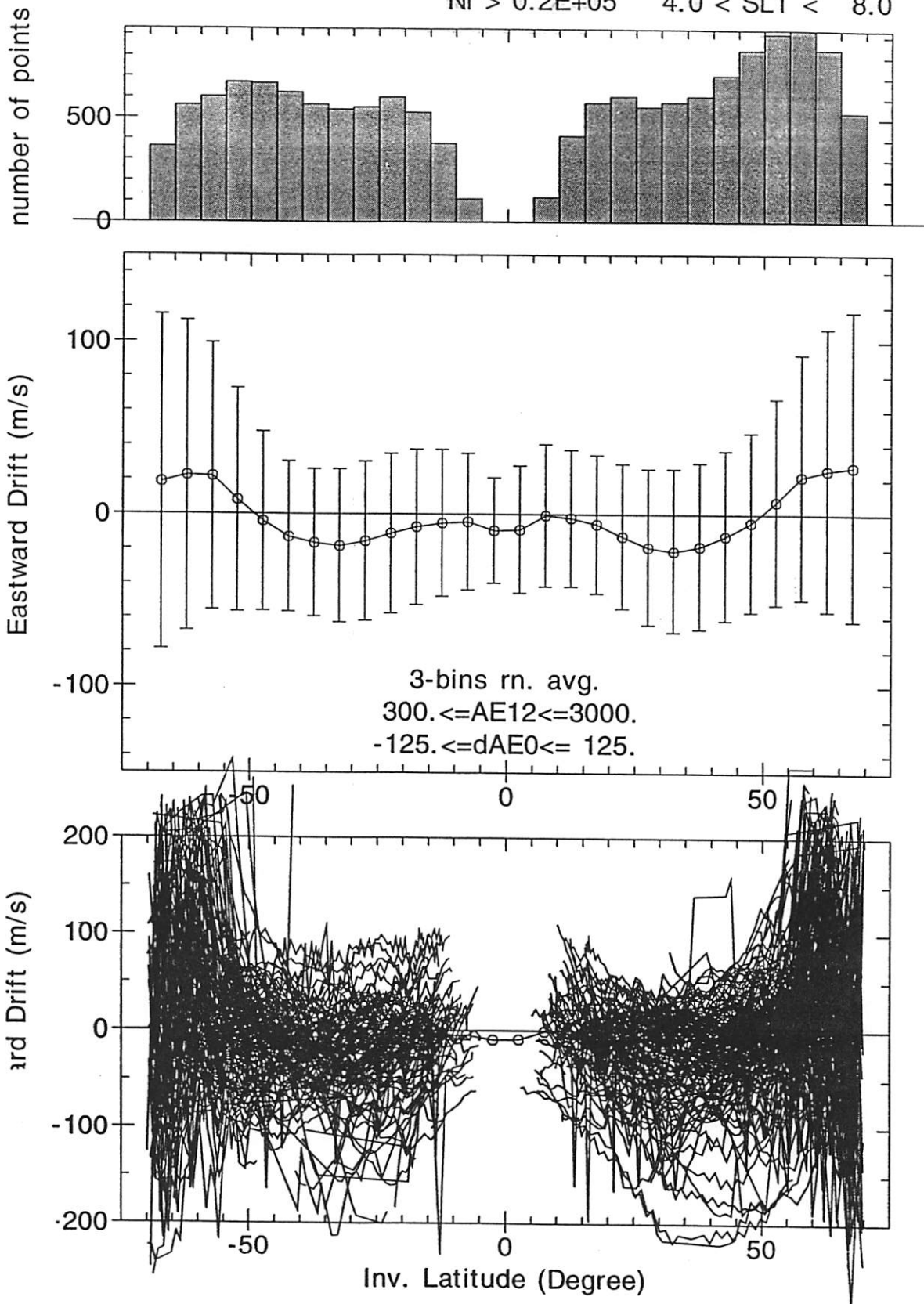
DE-2 81,82,83

200 < ALT < 800

Ni > 0.2E+05

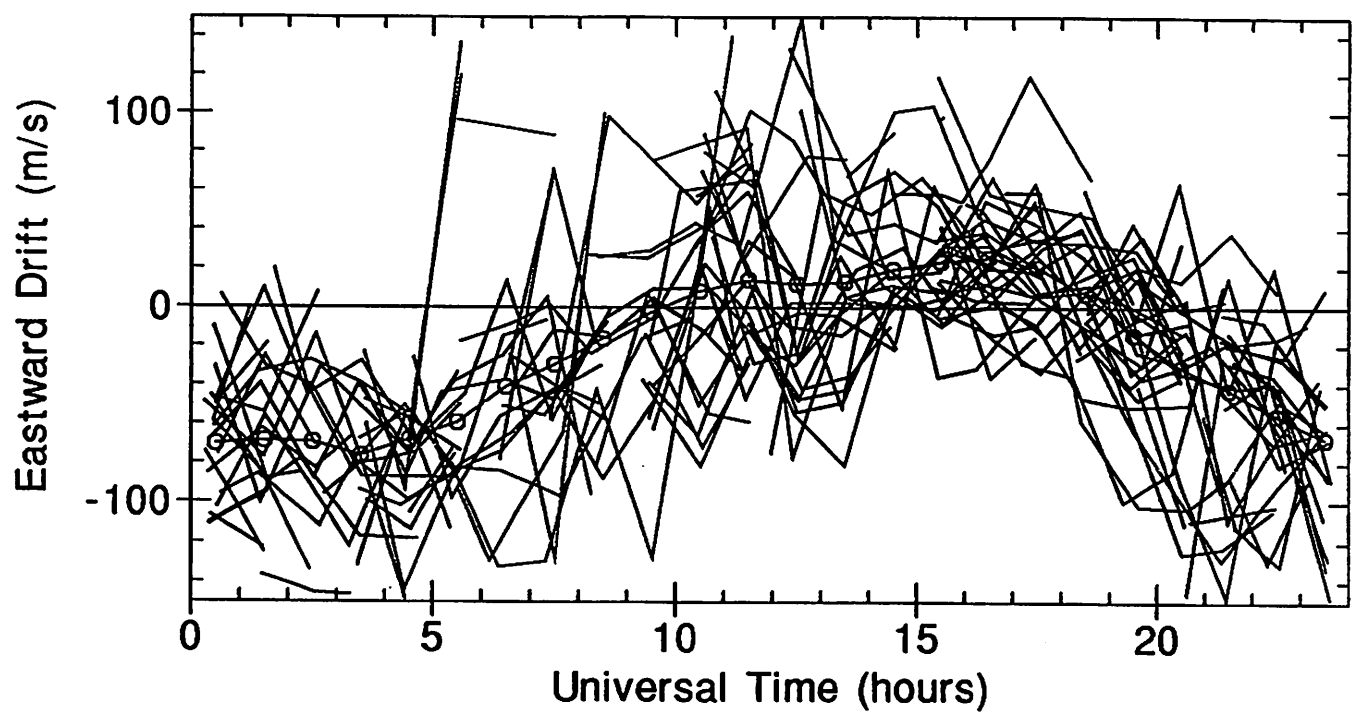
0 < GLON < 360

4.0 < SLT < 8.0



Millstone 1984-92
Equinoxes

$K_p \geq 3.0$
 $0. \leq \Phi \leq 500.$



DATA

- Over 200,000 (16 sec averaged) zonal drift observations from 15° to 60° invariant latitude from 280-800 km measured by the Ion Drift Meter on board of the DE-2 satellite.
- About 150 days of hourly averaged incoherent scatter radar observations of F-region plasma drifts from Arecibo and Millstone Hill.
- We use the AE index to characterize the disturbance level of the high latitude current system, and to estimate the polar cap potential drop and the global energy injection [e.g., Ahn *et al.* 1992, 1983] i.e.,

$$\Phi \text{ (kV)} = 36 + 0.082 \text{ AE (nT)}$$

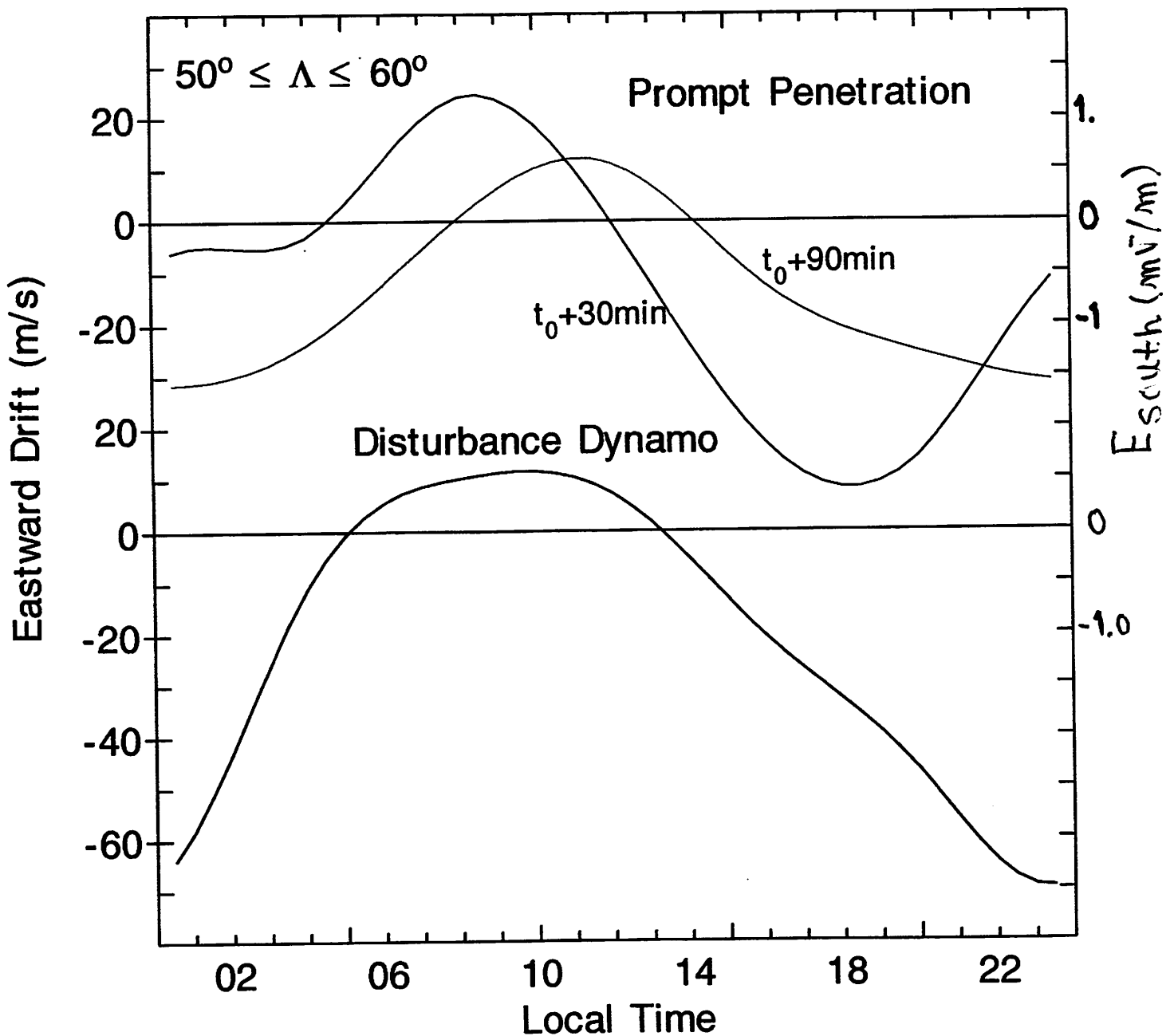
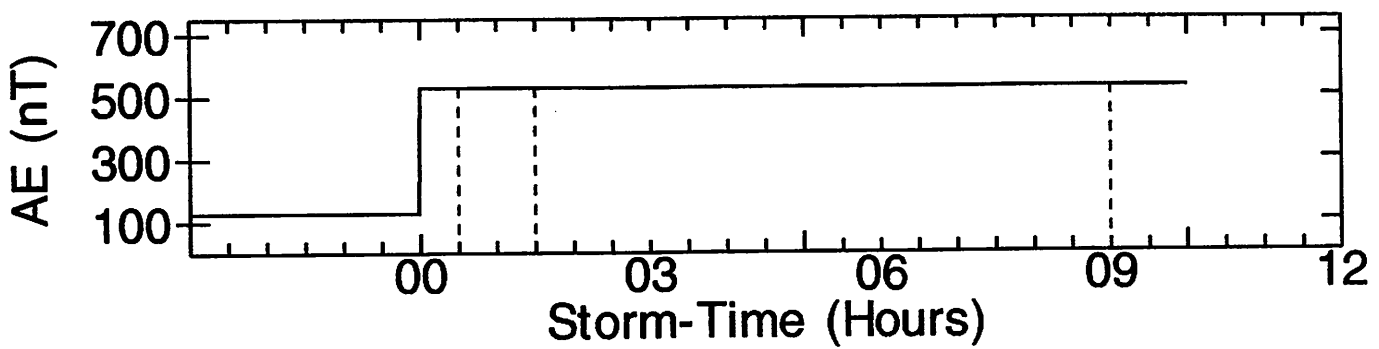
$$U(W) = 2.9 \times 10^9 \text{ AE (nT)}$$

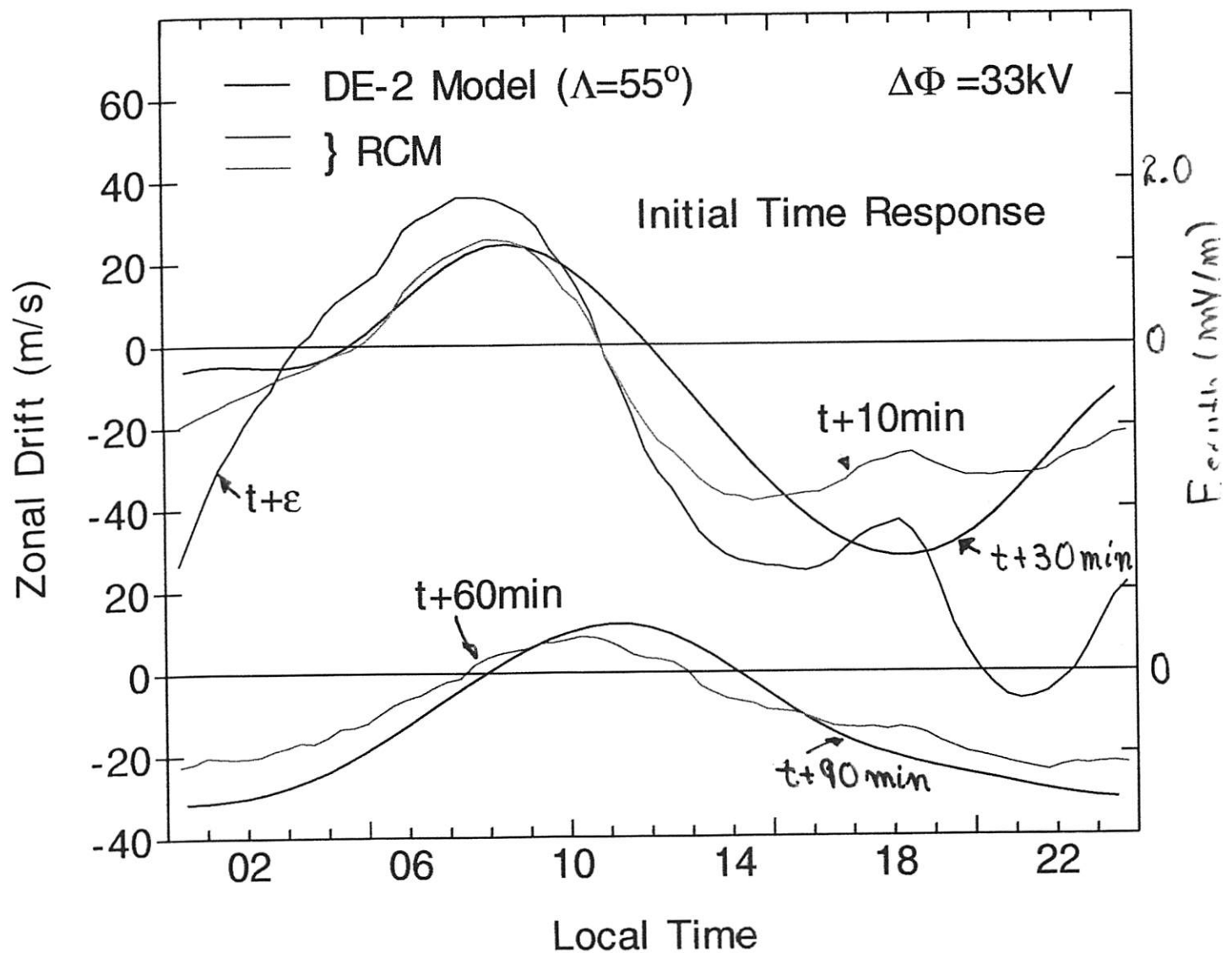
DE-2 Empirical Storm Time Model

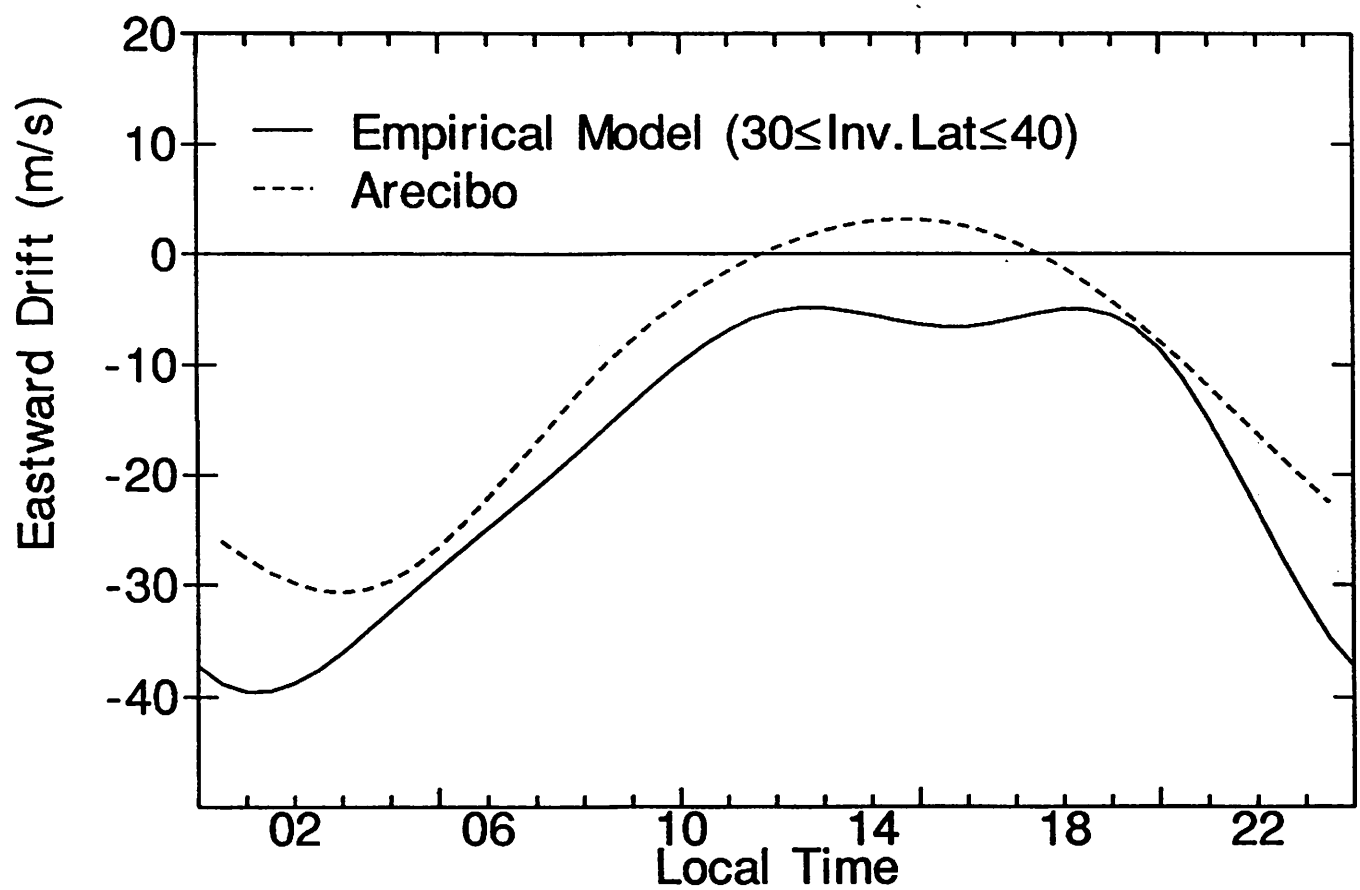
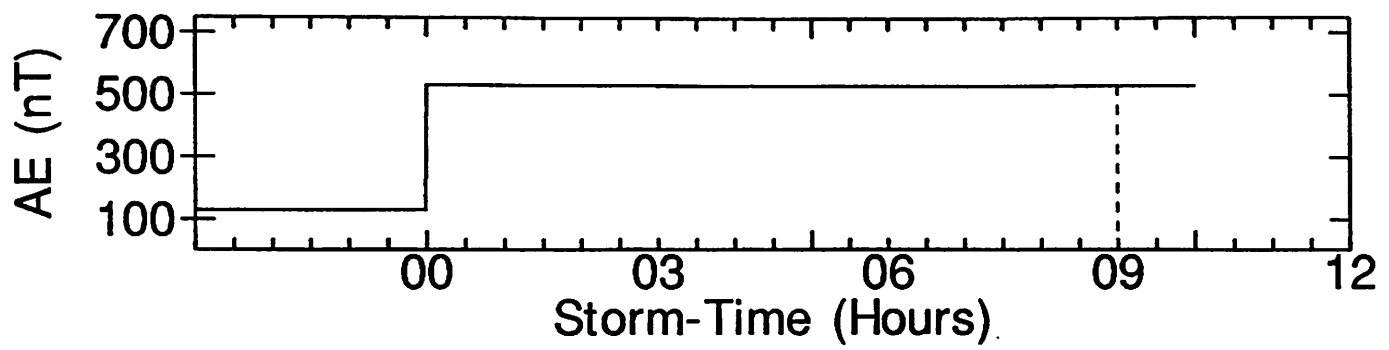
- Model allows for separation of prompt penetration and disturbance dynamo electric fields
- Based on 6 normalized cubic B-splines to describe local time dependence
- Model can be expressed as:

$$v(t, \Lambda) = \sum_{i=1}^6 [\underbrace{a_{i,1}(\Lambda) \Delta AE(t) + a_{i,2}(\Lambda) \Delta AE(t - 1\text{hr})}_{\text{prompt penetration}} + \underbrace{a_{i,3}(\Lambda) AE_d(1 - 9h)}_{\substack{\text{disturbance dynamo} \\ + \\ \text{Steady-state leakage}}}] N_{i,4}(t)$$

- Model-Coefficients were obtained by least squares fit using 10° overlapping latitudinal bins from 15° to 60° , where each bin contained more than 40,000 data points







Summary and Conclusions

- Incoherent scatter radar and satellite measurements have determined the average latitude dependent plasma drift (electric field) patterns during magnetically quiet and disturbed conditions but their longitudinal dependence is still not well understood.
- Longitudinal effects on the ionospheric plasma drifts are particularly important at equatorial latitudes where the plasma drift plays important roles on the distribution of ionization and on the generation of plasma instabilities.
- The ionospheric electric fields and plasma drifts exhibit large quiet-time variability particularly near solar minimum. The understanding of this variability is of fundamental importance for the development of realistic predictive models.
- We have determined the latitude dependent zonal plasma drift patterns resulting from magnetospheric dynamo and ionospheric disturbance dynamo electric fields during magnetically disturbed conditions.
- The perturbation drift patterns obtained from DE-2 satellite observations and from Millstone Hill and Arecibo incoherent scatter radar measurements are in good agreement.

- The short lived and steady-state components of the magnetospheric dynamo electric fields at middle and low latitude are in reasonably good agreement with results from the Rice Convection Model, and the disturbance dynamo electric field patterns are generally consistent with those from the Blanc-Richmond model.
- The ionospheric disturbance dynamo electric fields are fully developed 1-3 hours after step function changes in the polar cap potential drop. However, disturbed periods lasting longer than a few hours it is very difficult to fully decouple the perturbations due to disturbance dynamo electric fields and from the leakage of high latitude electric fields to lower latitudes.
- We are starting to study a number of processes (e.g., energy deposition in different local time sectors, By effects, electric fields associated with traveling atmospheric disturbances, temperature of the ions in the ring current) which affect the amplitude and phase of the middle and low latitude perturbation electric fields.
- The detailed understanding of ionospheric transport processes requires that of the coupling between plasma drifts and thermospheric neutral winds and use of multi-instrument studies and of numerical models. Multi-instrument studies require the careful considerations of the properties and limitations of the different measurement probes.